American Journal of Applied Sciences

Article

A Comparative Investigation of 2-Mercaptobenzothiazole and Na_2HPO_4 as Corrosion Inhibitors for API 5L X42 Pipeline Steel

Ioannis A. Kartsonakis, Panagiota Stamatogianni, Evangelia K. Karaxi and Costas A. Charitidis *

Research Unit of Advanced, Composite, Nano-Materials and Nanotechnology, School of Chemical Engineering, National Technical University of Athens, 9 Heroon Polytechniou St., Zographos, GR-15773 Athens, Greece;

Abstract: Mild or low-carbon steel has an increasing utilization and is widely used for building construction, machinery parts, and pipelines, because it can be machined easily and has enhanced weldability as well as a low price. In any case, the corrosion resistance of mild steel under the conditions in industrial applications or in atmosphere is a thoughtful concern. This study inquiries into the application of 2-mecraptobenzothiazole (MBT) and Na_2HPO_4 as corrosion inhibitors for the protection of API 5L X42 pipeline steel in 3.5 wt % NaCl as well as in water from the Athens city supply system. The electrochemical/morphological characterizations of the afore mentioned mild steel proved that the corrosion protection mechanisms can be assigned to the protective layers created onto the metal surface because of the presence of the inhibitors, which prevent chloride's penetration. The synergistic effect of the MBT and Na_2HPO_4 corrosion inhibition behavior, in a molar ratio of 1:1, revealed that the additives performed effectively with corrosion inhibition efficiency above 90%.

Keywords: mild steel; EIS; SEM; Raman spectroscopy; pitting corrosion; synergistic effect

1. Introduction

One of the most widespread kinds of steel is low-carbon or mild steel, not only for structural purposes but also for several applications in industry. Therefore, its usage and operation range from machinery parts, building materials, and domestic appliances to cutting tools, conveying tubes, cables, and magnets. Due to its low concentration in carbon (up to 0.29 wt %), mild steel exhibits extreme durability, great affordability, and significant mechanical, thermal, and magnetic properties [1–3]. Due to mild steel's increasing utilization, there has been great concern for the susceptibility of such steels caused by environmental corrosive factors, such as the humidity, acidity, or salinity of the atmosphere [4–6]. Thus, lots of studies have been focusing on low-alloy (weathering) steel corrosion and how to encounter it in a functional way [7–9].

In general, metallic corrosion is associated with any chemical alteration of the metal that stems from interaction with its environment [10]. Although intense research studies have taken place over all these decades to face corrosion, it still remains in the foreground since it is a continuous and inevitable process [11]. The main classification of corrosion types emphasized in the literature is between uniform and localized corrosion [12]. Pitting corrosion is a type of localized corrosion in which the metal is corroded in depth via the formation of indistinguishable pits. In the case of water and usually oil-conveying pipes, the corrosion effect often triggers uniform surface degradation internally, in parallel with localized corrosion underneath and oxide film formation [13,14]. Taking into account that pitting may cause the initiation of stress corrosion cracking [15], it is considered as the most detrimental corrosion effect. While uniform corrosion occurs during the subjection of mild steel in various environmental conditions [8,16], localized corrosion, such as pitting and scaling, takes place in the presence of heavy metal ions [17,18] or in locally high pH values [19]. Localized corrosion phenomena may thin locally the inner wall in a pipe, resulting in the creation of areas susceptible to cracking [20].

The protection of metallic materials from the corrosion effect could be achieved by intervening either in the alloy structure or in the alloy environment. The intervention in the alloy structure can be performed by changing the alloying ratio, by creating/applying metallic or organic coatings/films on the surface, by decreasing mechanical operation tensions, by the use of anodic or cathodic protection, and by adding corrosion inhibitors in the corroding solution [21]. In the literature, several studies indicate corrosion inhibition as an effective protection method [22,23]. A conventional classification of corrosion inhibitors is according to their inhibiting action. Therefore, there are adsorption inhibitors that undergo

chemisorption in the metallic surface, film-forming inhibitors, which are divided into passivation inhibitors (oxidizing or non-oxidizing) and precipitation inhibitors (deposition of three-dimensional film). However, the most common discrimination is between anodic, cathodic, and mixed-type inhibitors, considering which half-reaction they suppress during corrosion phenomena. Most organic inhibitors are of mixed-type and act as chemisorptive inhibitors. Phosphates act as cathodic inhibitors, whereas benzoates and azelates represent non-oxidizing film-forming inhibitors [24].

Concerning inorganic inhibitors, ideally the central atom of the inhibitor tends to form a complex entering the metallic lattice, without the need of additional energy and with the necessary stability [25]. Refaey et al. compared the inhibition ability of phosphate, chromate, molybdate, and nitrite as potential inhibitors for mild steel, in 0.1 M NaCl near neutral solutions. They concluded that phosphate demonstrated higher inhibition efficiency compared to the other inhibitors. Furthermore, phosphate deposited a strongly adherent layer, consisting of γ-Fe_2O_3 and $FePO_4 \cdot 2H_2O$, from the solution on the metal surface [26]. Regarding organic corrosion inhibitors, a perusal of the literature reveals a variety of organic compounds that have been suggested for encountering pitting corrosion on mild steel. An outstanding investigation was carried out by Marczewska-Boczkowska and Kosmulski using steel samples in aqueous solutions and indicating certain derivatives of azoles and thiazoles. They reported that imidazoles, benzothiazoles, and mercaptobenzothiazoles behaved as significantly efficient corrosion inhibitors against pitting. They claimed that these organic substances are capable of forming self-assembled monolayers, which improve inhibition and confer a protective layer of great stability, due to the spontaneous self-assembly process [27]. Moreover, Wang et al. synthesized and utilized an organic chemical compound, 4-salicylideneamino-3-phenyl-5-mercapto-1,2,4-triazole, as a corrosion inhibitor for mild steel, in electrolytic solution of 1 M HCl solution in several temperatures, which was based on the enhanced corrosion inhibition of the combined N and S elements in heterocyclic organic compounds [26]. They also pointed out that the presence of both elements functions more efficiently instead of the use of substances that contain only nitrogen or sulfur separately. This outcome was attributed to the combination of phenyl, mercapto, and azomethine reactive groups. Taking into account these claims, 2-mercaptobenzothiazole (MBT) was rendered as one of the most preferable mixed-type organic inhibitors for mild steel in aqueous solutions [28].

The self-assembling effect [29] and the chemisorption ability in conjunction with the aromatic nature of the inhibitor, which confers increased stability [25], lead to the need to investigate how to optimize inhibition by the use of MBT. Furthermore, its efficiency in near neutral aqueous solutions was taken into account. A common utilization of MBT was in coolant mixtures as a corrosion inhibitor for low-carbon steel pipes [30]. It exhibited improved inhibition efficiency when mixed with different organic inhibitors, denoting the advanced synergistic inhibition effect through smart combinations. Gunasekaran et al. evaluated the synergistic corrosion inhibition of several phosphonic acids substituting metal ions for azoles, provided that phosphorous inhibition ability could be exploited in chemically different systems [31]. A conventional use of phosphate anions in corrosion inhibitors is in cooling systems that maintain cavitation problems and intense corrosion phenomena [32]. Calmon et al. patented certain mixtures against pitting and the galvanic corrosion of copper and iron surface, consisting of sodium phosphates (Na_2HPO_4) or polyphosphates ($Na_2P_4O_{13}$) synergistically with sodium mercaptobenzothiazole in aqueous solutions emphasizing the immediate connection between inhibition efficiency and inhibitor concentration [33].

The aim of this study is to investigate the susceptibility of mild steel to corrosion in industrial hot/cooling systems after its exposure in 3.5 wt % NaCl as well as in the water of the Athens city supply system. The main goal of the presented experiments is to identify which inhibitors perform best at restricting the aforementioned corrosion process. The importance of these experiments is directly linked to the current urgent need for industrial mild steel pipeline corrosion protection.

In this regard, the protection effectiveness of the complexes, oxides, or salts that are created on the mild steel surface, as well as the morphological conversions that occur on the surface of the metal alloy panels following exposure in the presence or absence of MBT and Na_2HPO_4, were evaluated by three families of techniques: electrochemical, microscopy, and spectroscopy. The electrochemical characterization demonstrated that MBT and Na_2HPO_4 can be considered as corrosion inhibitors of mild steel as they reduced the corresponding anodic and/or cathodic corroding reactions. Moreover, the synergistic effect of the corrosion inhibition behavior of MBT and Na_2HPO_4 in a molar ratio 1:1 at several concentrations was studied. The analysis revealed that the admixtures performed effectively with inhibition efficiency above 90%. The presence of both aforementioned inhibitors into the corrosive environment exhibited the highest impedance modulus (|Z|) and polarization resistance (R_p) value as the exposure time elapsed.

Regarding the X-ray diffraction (XRD) measurements and scanning electron microscopy (SEM) characterization, it was disclosed that the exposure of mild steel to a corrosive environment in the presence or absence of inhibitors resulted in the creation of several oxide, hydroxide, and hydroxide–phosphate compounds on the steel surface. According to the aforementioned characterization techniques,

the corrosion protection mechanisms of steel can be ascribed to the protective films created onto the metal surface because of the inhibitors' presence, which prevent chlorides' insertion. The performed experiments shed light on the corrosion mechanisms of mild steel in industrial hot/cooling systems.

2. Materials and Methods

2.1. Reagents and Solutions

All the compounds and reagents were of analytical reagent grade. Sodium phosphate dibasic dihydrate ($Na_2HPO_4 \cdot 2H_2O$, Sigma-Aldrich) and 2-mercaptobenzothiazole (MBT, Sigma-Aldrich) were used without further purification. Hot-rolled black (non-galvanized) mild steel panels were manufactured by TMK-ARTROM S.A. and accompanied with all certifications required (ASTM A568/A568M-09 [34]). Electrochemical measurements were performed on mild steel grade API 5L X42 conveying a pipeline with the following chemical composition (wt %): C: 0.15, Mn: 0.56, S: 0.002, P: 0.12, Si: 0.21, Ni: 0.07, Cr: 0.04, Mo: 0.01, Cu: 0.22, Al: 0.020, N: 0.009, V+Ti+Nb: 0.004, and Fe
as remainder.

2.2. Preparation of Substrates

The mild steel panels were abraded with SiC paper up to 5 μm grain size (P4000) and then cleaned in agreement with ASTM D6386-99 (reapproved 2005) [35] prior to being used in the conducted experiments. This procedure is necessary because the exposed steel interacts with the environment to form several iron oxides such as α-FeO(OH), γ-FeO(OH), β-FeO(OH), and Fe_3O_4 [36]. According to the aforementioned standard, the cleaning procedure includes the degreasing of steel panels with their subjection in a mixture of acetone and ethanol (50:50) of purity 96% *v*/*v* for about 20 min, and then their exposure to NaOH solution of pH 11 for 5 min at 60 °C. Finally, the panels are rinsed with distilled water and dried in a desiccator in order to avoid the formation of new corrosion products, as uncoated black mild steel is susceptible to corrosion by humidity, as analyzed above.

2.3. Characterization

Several imaging techniques providing information at macro- and microscopic scales were used in order to evaluate the surface morphology of the mild steel panels. The microscale information was collected with SEM imaging performance using a Hitachi Tabletop Microscope TM3030 Scanning Electron Microscopy equipped with an energy dispersive X-ray spectrophotometer (EDS) system (QUANTAX 70), and with an ultra-high resolution scanning electron microscopy (UHR-SEM) using NOVA NANOSEM 230 (FEI Company). The macroscale information with respect to optical details was acquired using a Samsung Galaxy A7 auto focus triple camera 24 MP + 5 MP + 8 MP. The chemical analysis was conducted via micro-Raman measurements using a Renishaw inVia spectrometer working in backscattering configuration and equipped with a near-infrared diode laser emitting at 532 and 785 nm. The spectra were recorded by focusing the laser beam on the sample surface and adjusting the light power so that 1 mW was provided for a spot of about 1 μm diameter. The compounds that are created on the subjected mild steel panels were studied via XRD measurements. The crystal structure was identified by powder X-ray diffraction using an X Bruker D8 Advance Twin Twin, employing Cu–Kα radiation (λ = 1.5418 Å).

The electrochemical characterizations based on linear polarization resistance (LPR) and potentiodynamic polarization (PP) were conducted using a VersaSTAT 3 Potentiostat/Galvanostat/Frequency Response Analyzer instrument (Princeton Applied Research, AMETEK). Concerning the PP measurements, a three-electrode electrochemical cell was used, consisting of a saturated silver chloride electrode [$Ag/AgCl,KCl_{(sat)}$] as reference, a working electrode (≈1.0 cm^2 of exposed area), and a platinum foil as counter electrode. The assessment of the polarization curves on the bare alloy was accomplished after different exposure intervals. Cathodic and anodic branches of polarization curves were recorded separately with the potential scan rate of 1 mVs^{-1} in the cathodic and in the anodic directions, starting from the open circuit potential (OCP, E_{OC}, corrosion potential), at room temperature. Regarding the LPR measurements, the scan rate was 0.1 mVs^{-1} and the potential range was ± 2.5 mV versus OCP. The R_p (polarization resistance) is the definition of the ratio of the applied potential to the applied current ($\Delta E/\Delta I$). The slope of the potential versus current plot is used for the calculation of the R_p [37]. The R_p denotes the degree of the specimen susceptibility to be corroded [38,39]. The corrosion protection performance of the inhibitors was estimated via electrochemical impedance spectroscopy (EIS). The EIS measurements were conducted using the aforementioned potentiostat instrument with the arrangement of the three-

electrode electrochemical cell, in a frequency range from 10 μHz to 1 MHz. All spectra were recorded at open circuit potential, applying a 10 mV sinusoidal perturbation (rms signal) at room temperature. During all measurements, the electrochemical cell was placed in a Faraday cage. The Z-view Software (Scribner Associates Incorporated, SAI) was used for the analysis of the obtained spectra utilizing the adequate equivalent electric circuits. Two different types of electrolytic solutions (300 mL) were used: (i) water from the supply system of Athens city (WSS: water of the Athens city supply system after a softening process, Table 1), and (ii) 3.5 wt % NaCl solution prepared in distilled water [ASTM G44-99 (2013)] [40].

Table 1. Ion composition of the water of the Athens city supply system after a softening process (WSS) estimated via atomic absorption spectroscopy (mg/L).

K	Ca	Mg	Fe	Mn	Zn
1.7733	0.346	0.09755	1.36	0.005	0.0052

Moreover, the corrosion phenomena on a metallic uncoated surface was further evaluated with respect to the influence of corrosion inhibitors. Consecutively, 6 mM electrolytic solutions of the impending corrosion inhibitors were prepared for each compound as well as certain equimolecular 6 mM solutions of both Na_2HPO_4 and MBT for the investigation of their synergistic inhibition effect (Table 2). The sample *Steel-blank* is ascribed to mild steel panel prior to subjection in electrolytic solutions.

Table 2. Composition of the solutions for testing the effectiveness of the inhibitors onto mild steel. Reagents concentration 6 mM, reagents solubility in water (mg/100 g, 20 °C) 1.7×10^3 Na_2HPO_4, 1.9×10^1 MBT.

Composition	pH	Sample
-	-	*Steel–blank*
WSS	7.41–7.52	*Steel–WSS–blank*
WSS + 0.849 g/L Na_2HPO_4	7.78–7.97	*Steel–WSS–Na_2HPO_4*
WSS + 1.014 g/L MBT	7.33–7.52	*Steel–WSS–MBT*
WSS + 0.849 g/L Na_2HPO_4 + 1.014 g/L MBT	7.38–7.82	*Steel–WSS–Na_2HPO_4–MBT*
NaCl 3.5 wt %	7.71–7.72	*Steel–NaCl–blank*
NaCl 3.5 wt % + 0.849 g/L Na_2HPO_4	7.78–7.97	*Steel–NaCl–Na_2HPO_4*
NaCl 3.5 wt % + 1.014 g/L MBT	7.33–7.52	*Steel–NaCl–MBT*
NaCl 3.5 wt % + 0.849 g/L Na_2HPO_4 + 1.014 g/L MBT	7.38–7.82	*Steel–NaCl–Na_2HPO_4–MBT*

The corrosion inhibition efficiency, η(%), was estimated by Equation (1):

$$\eta(\%) = \frac{R_{ct(inhibitor)} - R_{ct(bareMetal)}}{R_{(inhibitor)}} \times 100 \quad (1)$$

where $R_{ct(inhibitor)}$ and $R_{ct(bareMetal)}$ represent the charge transfer resistances in the presence and in the absence of an inhibitor, respectively [41,42].

The synergistic parameter (S_i) was calculated from Equation (2) given by Aramaki and Hackerman [43]:

$$S_i = \frac{1 - \eta_{1+2}}{1 - \eta^*_{1+2}}, \quad (2)$$

where η_1 is the inhibition efficiency of the Na_2HPO_4, η_2 is the inhibition efficiency of the MBT, and $\eta_{1+2} = (\eta_1 + \eta_2) - (\eta_1 \times \eta_2)$, η^*_{1+2} is the measured inhibition efficiency of the MBT in combination with

3. Results and Discussion

3.1. Morphology Evaluation

The visual pictures of mild steel immersed in WSS for 96 h, in the presence of inhibitors or not, are demonstrated in Figure 1a–d. Onto the slightly rinsed corroded surface of Figure 1a, ferrous yellowish, orange, and brownish red species create a hardly homogenous layer, as expected from the literature for the mild steel surface in the absence of inhibitors (*Steel–WSS–blank*). Susceptible to a series of local corrosion phenomena as well as to the creation of local galvanic cells and pits, the final layer emerges in dependence with the local composition and physicochemical conditions of the system [44]. In depth, it is claimed that reddish hues stem from hematite (α-Fe_2O_3) in a hexagonal crystal system, in which the face-sharing octahedral keeps the Fe centers at the shortest distance (0.29 nm), whereas the yellowish ones are caused by the edge- or/and corner-sharing octahedral of lepidocrocite [γ-FeO(OH)], maghemite (γ-Fe_2O_3), goethite [α-FeO(OH)] and other compounds, with Fe center distances from
0.30 to 0.35 nm. In the presence of each inhibitor separately, the mild steel surface is either converted by the phosphate invasion into the crystal lattice, in case of phosphate solution in *Steel–WSS–Na_2HPO_4* (Figure 1b), or covered by the organic three-dimensional organic layer precipitated, in the case of MBT in *Steel–WSS–MBT* (Figure 1c). In mere phosphate solutions, the lack of reddish corrosion products and the development of a thinner and yellower final layer, as shown in Figure 1b (*Steel–WSS–Na_2HPO_4*) and Figure 1f (*Steel–NaCl–Na_2HPO_4*), are characteristic of the corrosion process due to the hindrance of hematite formation, as detailed below. Since the earlier stages and according to the literature, the inner layer (2D layer) is expected to consist of gray and blackish magnetite (Fe_3O_4) and maybe wustite (FeO). Supplementary to the electrochemical and spectroscopic measurement analyses that are discussed in detail below, the visual image of Figure 1d confirms the synergistic action of the inhibitors (*Steel–WSS–Na_2HPO_4–MBT*), overcoming the defects and enhancing the advantages of the preceded separate use of MBT and Na_2HPO_4. After the exposure tests, a compact, resistant, uniform, protective layer was created, appearing to have a light-colored saline coating in the outer and a metallic gray or blackish inner layer, which is the magnetite layer. At a first glance, the lack of brown, reddish, and yellowish hues in the corrosion products incline us toward the conception that the main and more time-consuming corrosion processes were restricted successfully, resulting in a resistant and adherent protective layer on mild steel, which was almost intact after 96 h of subjection in a slightly saline environment and even after drying.

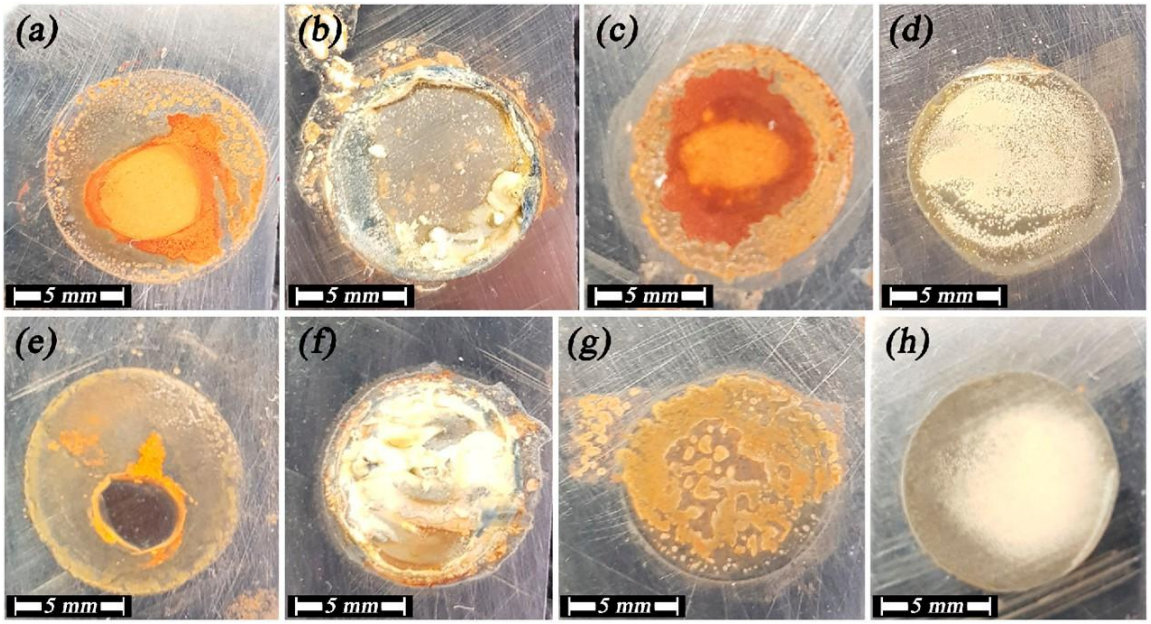

Figure 1. Visual images of mild steel after submission for 96 h: in WSS (**a**) *Steel–WSS–blank*, (**b**) *Steel–WSS–Na_2HPO_4*, (**c**) *Steel–WSS–MBT*, (**d**) *Steel–WSS–Na_2HPO_4–MBT*; in 3.5 wt % NaCl (**e**) *Steel–NaCl–blank*, (**f**) *Steel–NaCl–Na_2HPO_4*, (**g**) *Steel–NaCl–MBT*, (**h**) *Steel–NaCl–Na_2HPO_4–MBT*.

The mild steel visual pictures after exposure to 3.5 wt % NaCl for 96 h, in the presence or absence of inhibitors, are illustrated in Figure 1e–h. It can be seen that the surface of mild steel without the influence of inhibitors has lots of corrosion signs, as it is the bluish gray stain, indicating

that uniform and local corrosion phenomena took place, with an accelerated rate regarding to the blank system (*Steel–NaCl–blank*, Figure 1e). On the other hand, corrosion products are also observed on the surface of both *Steel–NaCl–*Na_2HPO_4 and *Steel–NaCl–MBT* (Figure 1f,g), reassuring that the chosen inhibitors are appropriate for the present system. Moreover, the surface of the sample with the presence of both inhibitors seems free from corrosion products in the outer area and a more compact, dark-colored adherent layer onto the metallic surface was developed, with brown-gray color, which was probably brown due to the organic tail of MBT and blackish/gray due to magnetite and/or wustite compounds, as will be discussed below (*Steel–NaCl–*Na_2HPO_4*–MBT*, Figure 1h) [45].

The SEM images of mild steel prior to exposure to electrolytes (*Steel–blank*) are illustrated in Figure 2. It can be seen that there are holes, dents, and scratches on the surface either due to the fabrication of the specimens or due to the cleaning process. Taking into account the EDS analysis, the iron value concentration was measured to be approximately 92.9 wt %, while the corresponding oxygen value was estimated very low, roughly 0.1 wt % indicating the absence of iron oxide products (Table 3).

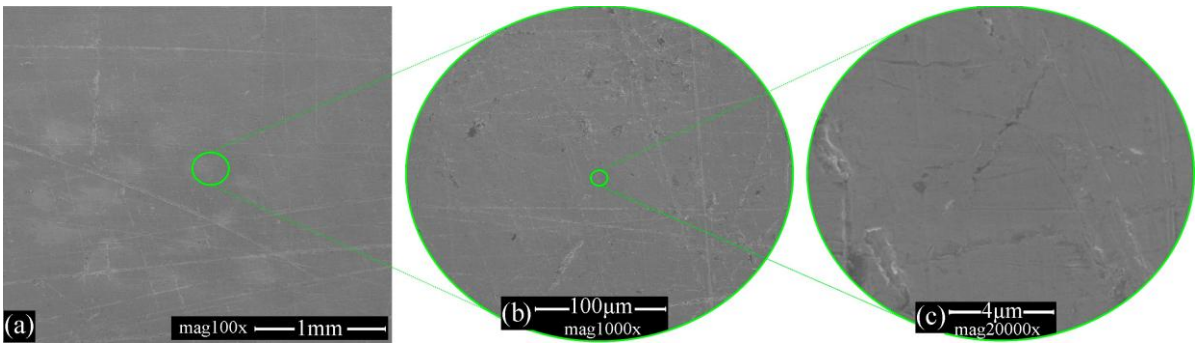

Figure 2. SEM images of mild steel prior exposure to electrolytes (*Steel–blank*).

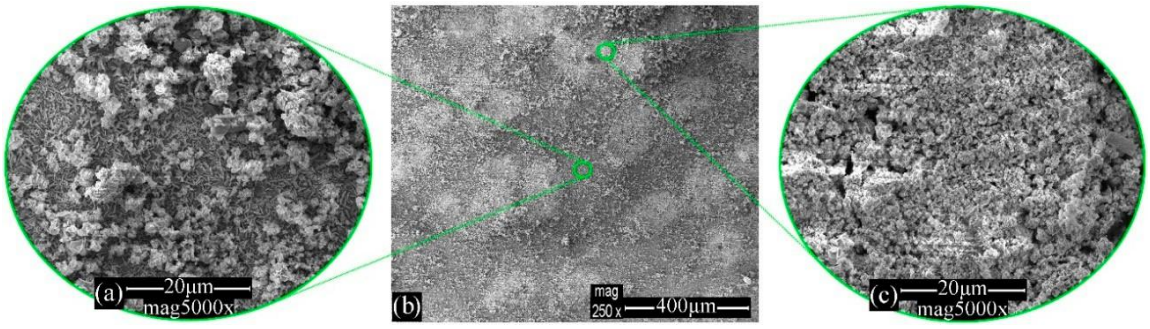

Figure 3. SEM images of mild steel immersed in WSS for 96 h in the absence of inhibitors.

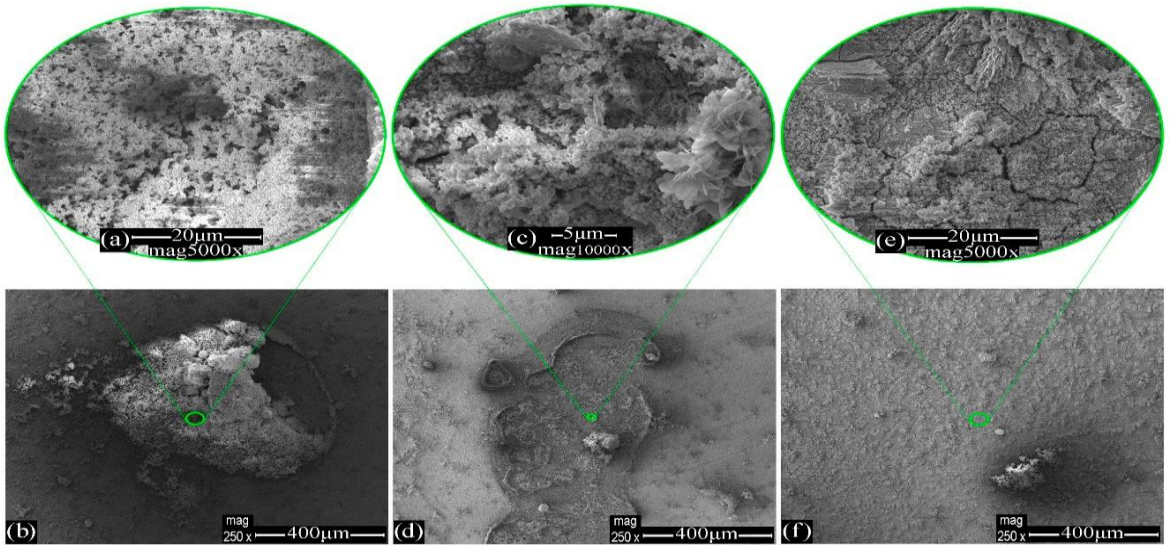

Figure 4. SEM images of mild steel immersed in WSS for 96 h in the presence of Na_2HPO_4.

Table 3. Tabulated values of wt % element concentration of mild steel panels prior and after subjection in either WSS, or 3.5 wt % NaCl for 96 h in the presence of inhibitors or not.

Sample	Spectrum at	wt % Element Concentration						
		O	Fe	C	Si	P	S	Na
Steel–blank	Figure 2a	0.1	92.9	3.7	2.0	-	-	-
Steel–WSS–blank	Figure 3b	52.3	44.0	1.5	2.3	-	-	-
Steel–WSS–Na_2HPO_4	Figure 4b	39.9	39.5	2.6	0.2	14.2	-	2.4
	Figure 4f	16.9	72.4	3.0	1.7	2.7	-	2.3
Steel–WSS–MBT	Figure 5e	44.6	46.1	4.2	1.2	-	3.6	-
	Figure 5f	44.4	46.9	4.3	1.5	-	2.9	-
Steel–WSS–Na_2HPO_4–MBT	Figure 6c	31.2	40.0	7.8	0.4	11.3	3.6	2.6
Steel–NaCl–Blank	Figure 7e	61.3	38.7	-	-	-	-	-
Steel–NaCl–Na_2HPO_4	Figure 8b	39.3	39.0	3.0	0.3	14.9	-	-
	Figure 8d	35.5	49.9	3.3	0.1	6.5	-	3.0
Steel–NaCl–MBT	Figure 9b	23.0	67.4	4.7	1.5	-	2.2	-
Steel–Na	*Figure*	47.1	26.8	4.5	-	16.0	5.2	0.4

Figure 5. SEM images of mild steel immersed in WSS for 96 h in the presence of MBT.

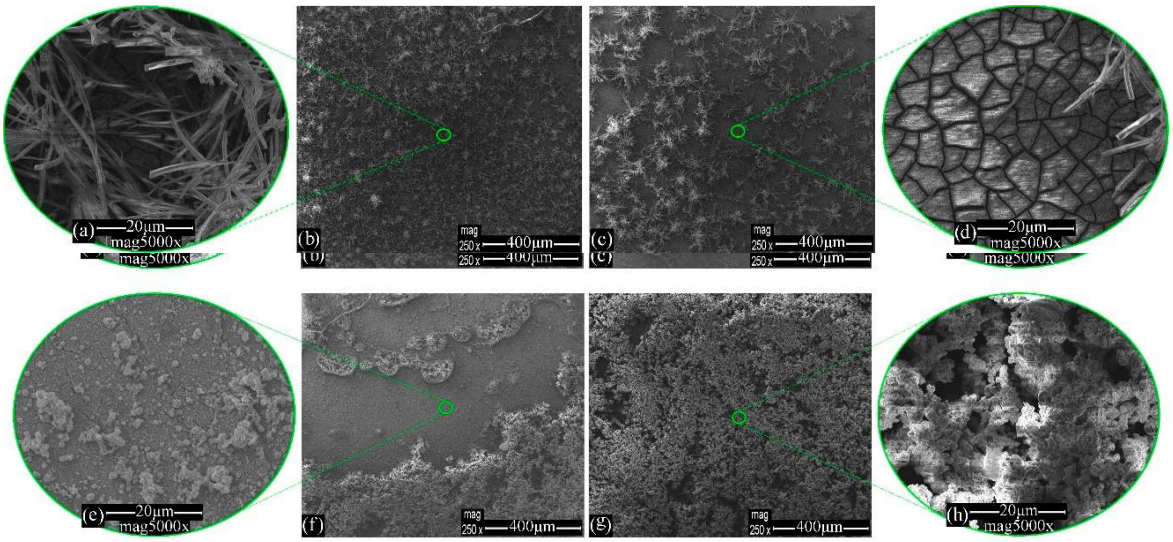

Figure 6. SEM images of mild steel immersed in WSS for 96 h in the presence of Na_2HPO_4 and 2-mecraptobenzothiazole (MBT).

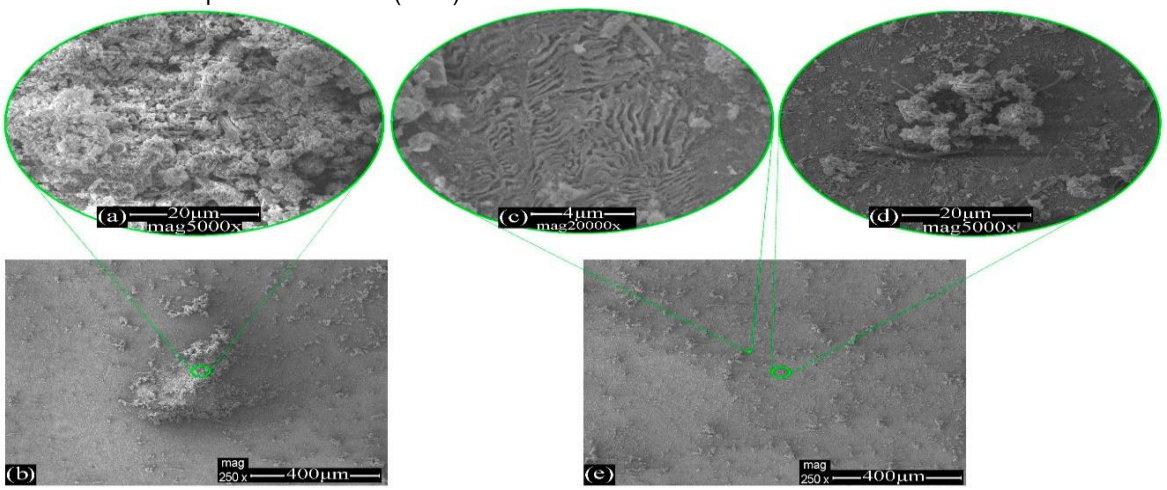

Figure 7. SEM images of mild steel immersed in 3.5 wt % NaCl for 96 h in the absence of inhibitors.

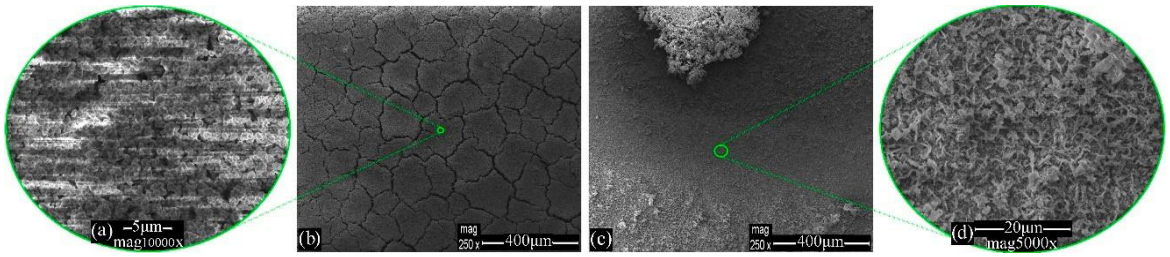

Figure 8. SEM images of mild steel immersed in 3.5 wt % NaCl for 96 h in the presence of Na_2HPO_4.

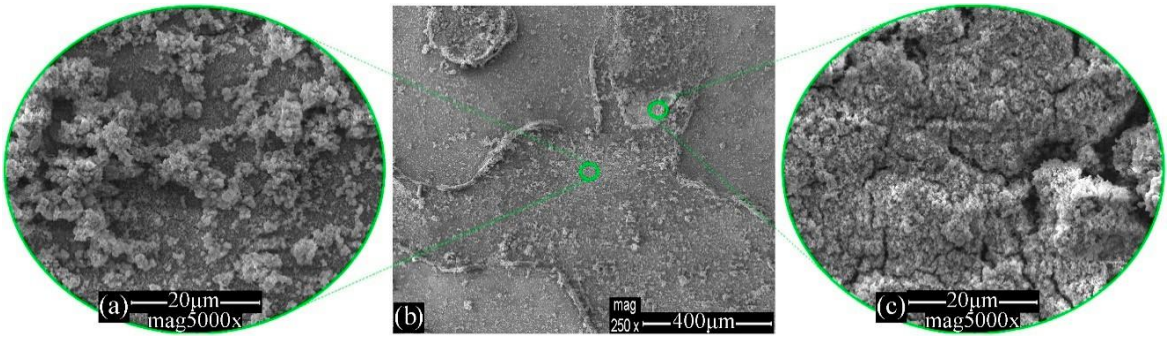

Figure 9. SEM images of mild steel immersed in 3.5 wt % NaCl for 96 h in the presence of MBT.

In general, the surface characterization of mild steel corrosion products remains a quite demanding issue, as denoted by previous works [46]. Various image analyzing techniques were deployed in order to assess the mild steel surface relating to its corrosion products structure and behavior after immersion in the studied inhibitor solutions.

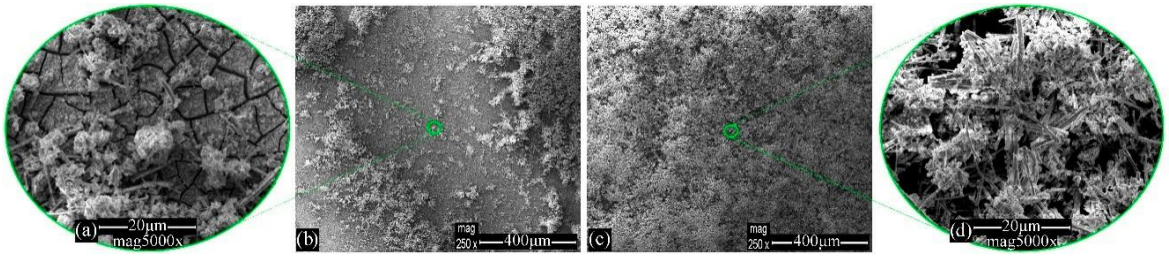

Figure 10. SEM images of mild steel immersed in 3.5 wt % NaCl for 96 h in the presence of Na_2HPO_4 + MBT.

In order to extract as much information as possible, it is a prerequisite to adopt a circumstantial model for the mild steel surface corrosion system during subjection in aquatic solutions, such as those proposed in the literature [7,47]. It is commonly accepted that the initial mixture of corrosion products consists of a primary viscous layer on a mild steel surface, to undergo afterwards gradation and separation into two distinguishable layers (an electrochemical double layer), an adherent rust layer, and a loosely adherent anodic oxide film [3,48]. At an early stage, amorphous masses of oxides with a spongy appearance are created, to transform primarily to lepidocrocite, part of which is further transformed in goethite. The studied phases have been generated either from the direct precipitation from a ferrous or a ferric solution, or by transformation of another iron oxide, at room temperature [3,49]. At a first glance at preceding investigations, Evan's model [50] regarding phase transition during wetting and drying conditions could contribute to illustrating the expended phase composition of a mild steel surface, after the prolonged exposure tests [51]. Consequently, during exposure, the reduction of lepidocrocite to a hydrated Fe^{2+}- intermediate takes place (phenomenon of olation) due to metal anodic dissolution, especially near the steel surface, where magnetite appears. However, oxidizing reactions can result in the emersion of lepidocrocite and maghemite phases [1,50,51] when oxygen circulation is evitable by drying [7].

The SEM images of mild steel immersed in WSS (*Steel–WSS–blank*) for 96 h, in the absence

of inhibitors, are illustrated in Figure 3. Characteristic laminar morphologies of lepidocrocite were captured on the reference sample surface, exhibiting a large spectrum of more or less known crystalline formations, as it is denoted in the literature. Near the mild steel surface broken glass type [3], flowery and worm nest shapes dominate, in parallel with the gradual growth of miscellaneous laminar volumes of lepidocrocite formed radially outward from the metal surface. This particular formation is also described by many as cotton balls [3] and defined as crystalline phases due to the aggregation of flat grains of lepidocrocite grown on top of amorphous γ-$Fe_2O_3 \cdot H_2O$ [46,48]. The EDS analysis of Figure 3b discloses enhanced oxygen value concentration compared to that of the *Steel–blank* sample due to the creation of the aforementioned iron oxides (Table 3).

The surface SEM images of *Steel–WSS–*Na_2HPO_4 after subjection in WSS for 96 h are depicted in Figure 4. It can be seen that characteristic tassel-like structures, mainly consisting of [Fe^{II}-OH] compounds, with substituted hydroxyls by phosphate anions ($H_2PO_4^-$, HPO_4^{2-}, PO_4^{3-}) [52], reveal the phosphates incorporation, thus making possible the identification of iron phosphates, appearing in amorphous or crystal phases. The latter are often observed as filamentous agglomerates [53] (Figure 4a,b). However, phosphorous detection through microscopy techniques of EDS analysis of the surface has been considered harsh, as phosphate anions get incorporated in steel crystal lattice [26]. Furthermore, ordinary structures of lepidocrocite spongy structure (and probably parts of maghemite, a phase that usually adopts the shape of its precursor [54]) and smaller aggregations of magnetite (as more globular, smooth) seem to be present, while a compact continuous inner layer (with cracks from drying process) has been obviously generated, which is indicative of steel surface passivation by phosphates (Figure 4c,d). In addition, large platy crystals of nanocrystalline phases are captured, reassuring the creation of the expected thin adherent passive layer of iron phosphates, maghemite, and lepidocrocite in crystalline and amorphous formations [26,53] (Figure 4e,f).

4. Conclusions

The electrochemical characterizations demonstrated that MBT and Na_2HPO_4 can be considered as corrosion inhibitors of steel. The initial mixture of corrosion products constitutes a primary viscous layer on the mild steel surface, which afterwards undergoes gradation and is separated into two distinguishable layers: an adherent rust layer and a loosely adherent anodic oxide film. At an early stage, amorphous masses of oxides with spongy appearance are created that transform chiefly to lepidocrocite, part of which is further transformed in goethite. During submission, the reduction of lepidocrocite to hydrated Fe^{2+} intermediate takes place due to metal anodic dissolution, especially near the steel surface, where magnetite appears. The chloride ions are considered to accelerate the corrosion process as aggressive anions, penetrating the protective layer and hence attacking the fresh unharmed metal surface beneath the layer, triggering pitting corrosion.

Adsorbed phosphate is assumed to act as a precursor for hematite creation and often for goethite nucleation and growth; at different concentrations and especially at locally more basic areas, phosphate anions increase the negative electronic charge of ferrihydrite (present at earlier stages) between particles, and therefore, the formation of hematite retards or is limited. The interaction of ions or neutral molecules at the electrical double layer changes its properties and structures. The water molecules pre-adsorbed at the metal surface in contact with the aqueous solution are involved in the successive adsorption processes. A thin multimolecular adsorption layer via the self-assembly process was formed (phosphonate layer formation) due to the intermolecular interaction between phosphonate groups. The inhibition mechanism is anodic type, hindering the active iron dissolution to a large extent. Since MBT contains polar groups with an atom of nitrogen and sulfur, the inhibiting properties were determined by the electron density at the reaction center. With an increase in the electron density at the reaction center, the chemisorption bonds between the MBT and the metal are strengthened. Therefore, MBT is adsorbed on the surface of mild steel, formatting stable produced self-assembled monolayers of MBT compounds on the surface of mild steel, protecting from aggressive ions. The inhibitive action of MBT takes place through the adsorption of its molecules onto the mild steel surface via the lone pair of electrons of the N and S atoms. The presence of both aforementioned inhibitors into the corrosive environment exhibited the highest impedance modulus and R_{ct} value as the exposure time elapsed. The synergistic effect of the corrosion inhibition behavior of MBT and Na_2HPO_4 in a molar ratio of 1:1 revealed that the admixture performed effectively with inhibition efficiency above 90% and with a synergistic parameter above 22. The synergistic effect of the corrosion inhibition behavior of MBT and Na_2HPO_4 is increased in the presence of NaCl due to the Cl^- interaction. Considering the electrochemical, spectroscopy, and morphology characterizations, the corrosion protection mechanisms of steel can be attributed to the protective layers formed onto the metal surface due to the presence of the inhibitors, which prevent chloride's penetration.

Author Contributions: I.A.K., P.S., and C.A.C. conceived and designed the experiments. P.S. and I.A.K. conducted the experiments. I.A.K., P.S., and E.K.K. performed the characterization and evaluation of the data. I.A.K., P.S., and C.A.C. discussed the data and wrote the paper. All authors have read and agreed to the published version of the manuscript.

Funding: This research received no external funding.

Conflicts of Interest: The authors declare no conflict of interest.

References

1. Evans, U.R.; Taylor, C.A.J. Mechanism of atmospheric rusting. *Corros. Sci.* **1972**, *12*, 227–246. [CrossRef]
2. Smith William, F.; Hashemi, J.; Wang, S.-H. *Foundations of Materials Science and Engineering*, 4th ed.; McGraw Hill: New York, NY, USA, 2006.
3. Raman, A.; Nasrazadani, S.; Sharma, L. Morphology of rust phases formed on weathering steels in various laboratory corrosion tests. *Metallography* **1989**, *22*, 79–96. [CrossRef]
4. Chen, Y.Y.; Tzeng, H.J.; Wei, L.I.; Wang, L.H.; Oung, J.C.; Shih, H.C. Corrosion resistance and mechanical properties of low-alloy steels under atmospheric conditions. *Corros. Sci.* **2005**, *47*, 1001–1021. [CrossRef]
5. Malaibari, Z.; Kahraman, R.; Saricimen, H.; Quddus, A. Investigation of atmospheric corrosion of mild steel after treatment by several inhibitor solutions. *Corros. Eng. Sci. Technol.* **2013**, *42*, 112–118. [CrossRef]
6. De la Fuente, D.; Díaz, I.; Simancas, J.; Chico, B.; Morcillo, M. Long-term atmospheric corrosion of mild steel. *Corros. Sci.* **2011**, *53*, 604–617. [CrossRef]
7. Allam, I.M.; Arlow, J.S.; Saricimen, H. Initial stages of atmospheric corrosion of steel in the Arabian Gulf. *Corros. Sci.* **1991**, *32*, 417–432. [CrossRef]
8. Kamimura, T.; Hara, S.; Miyuki, H.; Yamashita, M.; Uchida, H. Composition and protective ability of rust layer formed on weathering steel exposed to various environments. *Corros. Sci.* **2006**, *48*, 2799–2812. [CrossRef]
9. Morcillo, M.; Chico, B.; Díaz, I.; Cano, H.; de la Fuente, D. Atmospheric corrosion data of weathering steels. A review. *Corros. Sci.* **2013**, *77*, 6–24. [CrossRef]
10. Kolotyrkin, Y.M. Third International Congress on Metallic Corrosion. *Br. Corros. J.* **2013**, *1*, 89. [CrossRef]
11. Siddique, M.; Anwar-ul-Islam, M.; Butt, N.M.; Hussain, N.; Rehman, S.; Arshed, M. Mössbauer study of corrosion of mild steel induced by acid rain. *J. Radioanal. Nucl. Chem.* **1999**, *241*, 239–240. [CrossRef]
12. Migneault, S.; Koubaa, A.; Perré, P.; Riedl, B. Effects of wood fiber surface chemistry on strength of wood–plastic composites. *Appl. Surf. Sci.* **2015**, *343*, 11–18. [CrossRef]
13. McCafferty, E. *Surface Chemistry of Aqueous Corrosion Processes*; Springer: New York, NY, USA, 2015. [CrossRef]
14. Sha, W. *Steels: From Materials Science to Structural Engineering*; Springer: London, UK, 2013. [CrossRef]
15. Refait, P.; Génin, J.M.R. The transformation of chloride-containing green rust one into sulphated green rust two by oxidation in mixed Cl^- and SO_4^{2-} aqueous media. *Corros. Sci.* **1994**, *36*, 55–65. [CrossRef]
16. Parkins, R.N. The intergranular corrosion and stress corrosion cracking of mild steel in clarke's solution. *Corros. Sci.* **1994**, *36*, 2097–2110. [CrossRef]
17. Mobin, M.; Malik, A.U.; Andijani, I.N. The effect of heavy metal ions on the localized corrosion behavior of steels. *Desalination* **2007**, *217*, 233–241. [CrossRef]
18. Brinis, H.; Samar, M.E.H. A method for inhibiting scale formation and corrosion in a cooling water system. *Desalin. Water Treat.* **2013**, *52*, 2609–2619. [CrossRef]
19. Song, F.M. Predicting the mechanisms and crack growth rates of pipelines undergoing stress corrosion cracking at high pH. *Corros. Sci.* **2009**, *51*, 2657–2674. [CrossRef]
20. Eliyan, F.F.; Kish, J.R.; Alfantazi, A. Corrosion of New-Generation Steel in Outer Oil Pipeline Environments. *J. Mater. Eng. Perform.* **2016**, *26*, 214–220. [CrossRef]
21. Reeves, N.J.; Mann, S. Influence of inorganic and organic additives on the tailored synthesis of iron oxides. *J. Chem. Soc. Faraday Trans.* **1991**, *87*, 3875. [CrossRef]
22. Bockris, J.O.M.; Conway, B.E. Hydrogen Overpotential and the Partial Inhibition of the Corrosion of Iron. *J. Phys. Colloid Chem.* **1949**, *53*, 527–539. [CrossRef]
23. El Ibrahimi, B.; Jmiai, A.; Bazzi, L.; El Issami, S. Amino acids and their derivatives as corrosion inhibitors for metals and alloys. *Arab. J. Chem.* **2017**. [CrossRef]
24. McCafferty, E. *Introduction to Corrosion Science*; Springer Science: Washington, DC, USA, 2010. [CrossRef]
25. Sanyal, B. Organic compounds as corrosion inhibitors in different environments—A review. *Prog. Org. Coat.* **1981**, *9*, 165–236. [CrossRef]
26. Refaey, S.A.M.; Abd El-Rehim, S.S.; Taha, F.; Saleh, M.B.; Ahmed, R.A. Inhibition of chloride localized corrosion of mild steel by PO_4^{3-}, CrO_4^{2-}, MoO_4^{2-}, and NO^{2-} anions. *Appl. Surf. Sci.* **2000**, *158*, 190–196. [CrossRef]
27. Marczewska-Boczkowska, K.; Kosmulski, M. 2-Mercaptobenzothiazole as a Corrosion Inhibitor in Low

Temperature Ionic Liquids. In *Trends in Colloid and Interface Science XXIV*; Springer: Berlin/Heidelberg, Germany, 2011. [CrossRef]
28. Goudarzi, N.; Farahani, H. Investigation on 2-mercaptobenzothiazole behavior as corrosion inhibitor for 316-stainless steel in acidic media. *Anti Corros. Methods Mater.* **2013**, *61*, 20–26. [CrossRef]
29. Feng, Y.; Chen, S.; Zhang, H.; Li, P.; Wu, L.; Guo, W. Characterization of iron surface modified by 2-mercaptobenzothiazole self-assembled monolayers. *Appl. Surf. Sci.* **2006**, *253*, 2812–2819. [CrossRef]
30. Finšgar, M.; Jackson, J. Application of corrosion inhibitors for steels in acidic media for the oil and gas industry: A review. *Corros. Sci.* **2014**, *86*, 17–41. [CrossRef]
31. Gunasekaran, G.; Natarajan, R.; Muralidharan, V.S.; Palaniswamy, N.; Appa Rao, B.V. Inhibition by phosphonic acids—An overview. *Anti Corros. Methods Mater.* **1997**, *44*, 248–259. [CrossRef]
32. *Multicylinder Test Sequences for Evaluating Automotive Engine Oils: Sequence IID*; Sponsored by ASTM Committee B.01 on Automotive Lubricants and D-2 on Petroleum Products and Lubricants; American Society for Testing and Materials: West Conshohocken, PA, USA, 1993.
33. Heit, A.H.; Calvin, C. Corrusion Inhibition Compositions. U.S. Patent C 3, 291 C, 11 September 1962.
34. ASTM A568/A568M-09. *Standard Specification for Sheet, Carbon, Structural, and High-Strength, Low-Alloy, Hot-Rolled and Cold-Rolled, General Requirements for*; ASTM International: West Conshohocken, PA, USA, 2009. [CrossRef]
35. ASTM D6386-99. *Standard Practice for Preparation of Zinc (Hot-Dip Galvanized) Coated Iron and Steel Product and Hardware Surfaces for Painting*; ASTM International: West Conshohocken, PA, USA, 1999. [CrossRef]
36. Matsushima, I. Carbon Steel—Atmospheric Corrosion. In *Corrosion Handbook*; Revie, R.W., Ed.; John Wiley & Sons, Inc.: Hoboken, NJ, USA; Etobicoke, ON, Canada, 2008; pp. 515–528.
37. Kelly, R.G.; Scully, J.R.; Shoesmith, D.W.; Buchheit, R.G. The Polarization Resistance Method for Determination of Instantaneous Corrosion Rates. In *Electrochemical Techniques in Corrosion Science and Engineering*; Schweitzer, P.A., Ed.; Marcel Dekker, Inc.: New York, NY, USA, 2002; pp. 125–150.
38. Luo, X.; Ci, C.; Li, J.; Lin, K.; Du, S.; Zhang, H.; Li, X.; Cheng, Y.F.; Zang, J.; Liu, Y. 4-aminoazobenzene modified natural glucomannan as a green eco-friendly inhibitor for the mild steel in 0.5 M HCl solution. *Corros. Sci.* **2019**, *151*, 132–142. [CrossRef]
39. Fernandes, C.M.; Ferreira Fagundes, T.D.S.; Escarpini dos Santos, N.; Shewry de, M.; Rocha, T.; Garrett, R.; Borges, R.M.; Muricy, G.; Valverde, A.L.; Ponzio, E.A. Ircinia strobilina crude extract as corrosion inhibitor for mild steel in acid medium. *Electrochim. Acta* **2019**, *312*, 137–148. [CrossRef]
40. ASTM G44-99. *Standard Practice for Exposure of Metals and Alloys by Alternate Immersion in Neutral 3.5% Sodium Chloride Solution*; ASTM International: West Conshohocken, PA, USA, 2013. [CrossRef]
41. Migahed, M.A.; Al-Sabagh, A.M.; Khamis, E.A.; Zaki, E.G. Quantum chemical calculations, synthesis and corrosion inhibition efficiency of ethoxylated-[2-(2-{2-[2-(2-benzenesulfonylamino-ethylamino)-ethylamino] -ethylamino}-ethylamino)-ethyl]-4-alkyl-benzenesulfonamide on API X65 steel surface under H2S environment. *J. Mol. Liq.* **2015**, *212*, 360–371. [CrossRef]
42. Zhu, Y.; Free, M.L.; Yi, G. Electrochemical measurement, modeling, and prediction of corrosion inhibition efficiency of ternary mixtures of homologous surfactants in salt solution. *Corros. Sci.* **2015**, *98*, 417–429. [CrossRef]
43. Aramaki, K.; Hackerman, N. Inhibition Mechanism of Medium-Sized Polymethyleneimine. *J. Electrochem. Soc.* **1969**, *116*, 568. [CrossRef]
44. Tamura, H. The role of rusts in corrosion and corrosion protection of iron and steel. *Corros. Sci.* **2008**, *50*, 1872–1883. [CrossRef]
45. Revie, R.W. (Ed.) *Uhlig's Corrosion Handbook*; John Wiley & Sons: Hoboken, NJ, USA, 2011. [CrossRef]
46. Alcántara, J.; Chico, B.; Simancas, J.; Díaz, I.; de la Fuente, D.; Morcillo, M. An attempt to classify the morphologies presented by different rust phases formed during the exposure of carbon steel to marine atmospheres. *Mater. Charact.* **2016**, *118*, 65–78. [CrossRef]
47. Ma, Y.; Li, Y.; Wang, F. The effect of β-FeOOH on the corrosion behavior of low carbon steel exposed in tropic marine environment. *Mater. Chem. Phys.* **2008**, *112*, 844–852. [CrossRef]
48. Misawa, T.; Hashimoto, K.; Shimodaira, S. The mechanism of formation of iron oxide and oxyhydroxides in aqueous solutions at room temperature. *Corros. Sci.* **1974**, *14*, 131–149. [CrossRef]
49. De la Fuente, D.; Díaz, I.; Alcántara, J.; Chico, B.; Simancas, J.; Llorente, I.; García-Delgado, A.; Jiménez, J.A.; Adeva, P.; Morcillo, M. Corrosion mechanisms of mild steel in chloride-rich atmospheres. *Mater. Corros.* **2016**, *67*, 227–238. [CrossRef]
50. Evans, U.R. Mechanism of rusting. *Corros. Sci.* **1969**, *9*, 813–821. [CrossRef]
51. Stratmann, M.; Bohnenkamp, K.; Engell, H.J. An electrochemical study of phase-transitions in rust layers. *Corros. Sci.* **1983**, *23*, 969–985. [CrossRef]
52. Mathew, V.; Kim, S.; Kang, J.; Gim, J.; Song, J.; Baboo, J.P.; Park, W.; Ahn, D.; Han, J.; Gu, L.; et al. Amorphous iron phosphate: Potential host for various charge carrier ions. *NPG Asia Mater.* **2014**, *6*, e138. [CrossRef]
53. Tiwari, A.; Hihara, L.; Rawlins, J. (Eds.) *Intelligent Coatings for Corrosion Control*; Butterworth-

Heinemann: Oxford, UK, 2015. [CrossRef]
54. Cornell, R.M.; Schwertmann, U. *The Iron Oxides: Structure, Properties, Reactions, Occurrences and Uses*, 2nd ed.; Wiley-VCH Verlag GmbH & Co. KGaA: Weinheim, Germany, 2003.
55. Farzanian, K.; Pimenta Teixeira, K.; Perdigão Rocha, I.; De Sa Carneiro, L.; Ghahremaninezhad, A. The mechanical strength, degree of hydration, and electrical resistivity of cement pastes modified with superabsorbent polymers. *Constr. Build. Mater.* **2016**, *109*, 156–165. [CrossRef]
56. Gálvez, N. Effect of Phosphate on the Crystallization of Hematite, Goethite, and Lepidocrocite from Ferrihydrite. *Clays Clay Miner.* **1999**, *47*, 304–311. [CrossRef]
57. Schwertmann, U. Effect of pH on the Formation of Goethite and Hematite from Ferrihydrite. *Clays Clay Miner.* **1983**, *31*, 277–284. [CrossRef]
58. Antunes, R.A.; Costa, I.; Faria, D.L.A.D. Characterization of corrosion products formed on steels in the first months of atmospheric exposure. *Mater. Res.* **2003**, *6*, 403–408. [CrossRef]
59. Labinger, J.A. Bond-stretch isomerism: A case study of a quiet controversy. *C. R. Chim.* **2002**, *5*, 235–244. [CrossRef]
60. Tamilselvi, M.; Kamaraj, P.; Arthanareeswari, M.; Devikala, S.; Selvi, J.A. Development of nano SiO_2 incorporated nano zinc phosphate coatings on mild steel. *Appl. Surf. Sci.* **2015**, *332*, 12–21. [CrossRef]
61. Dwivedi, D.; Lepková, K.; Becker, T. Carbon steel corrosion: A review of key surface properties and characterization methods. *RSC Adv.* **2017**, *7*, 4580–4610. [CrossRef]
62. De la Fuente, D.; Alcántara, J.; Chico, B.; Díaz, I.; Jiménez, J.A.; Morcillo, M. Characterisation of rust surfaces formed on mild steel exposed to marine atmospheres using XRD and SEM/Micro-Raman techniques. *Corros. Sci.* **2016**, *110*, 253–264. [CrossRef]
63. Simard, S.; Odziemkowski, M.; Irish, D.E.; Brossard, L.; Ménard, H. In situ micro-Raman spectroscopy to investigate pitting corrosion product of 1024 mild steel in phosphate and bicarbonate solutions containing chloride and sulfate ions. *J. Appl. Electrochem.* **2001**, *31*, 913–920. [CrossRef]
64. Dhaiveegan, P.; Elangovan, N.; Nishimura, T.; Rajendran, N. Weathering Steel in Industrial-Marine-Urban Environment: Field Study. *Mater. Trans.* **2016**, *57*, 148–155. [CrossRef]
65. Sandhyarani, N.; Skanth, G.; Berchmans, S.; Yegnaraman, V.V.; Pradeep, T. A Combined Surface-Enhanced Raman-X-ray Photoelectron Spectroscopic Study of 2-mercaptobenzothiazole Monolayers on Polycrystalline Au and Ag Films. *J. Colloid Interface Sci.* **1999**, *209*, 154–161. [CrossRef]
66. Socrates, G. *Infrared and Raman Characteristic Group Frequencies*, 3rd ed.; John Wiley & Sons Ltd.: Chichester, UK, 2001; pp. 283–327.
67. De Faria, D.L.A.; Venâncio Silva, S.; de Oliveira, M.T. Raman microspectroscopy of some iron oxides and oxyhydroxides. *J. Raman Spectrosc.* **1997**, *28*, 873–878. [CrossRef]
68. Kolitsch, U.; Bernhardt, H.-J.; Lengauer, C.L.; Blass, G.; Tillmanns, E. Allanpringite, $Fe_3(PO_4)2(OH)_35H_2O$, a new ferric iron phosphate from Germany, and its close relation to wavellite. *Eur. J. Mineral.* **2006**, *18*, 793–801. [CrossRef]
69. Zhang, L.; Brow, R.K. A Raman Study of Iron-Phosphate Crystalline Compounds and Glasses. *J. Am. Ceram. Soc.* **2011**, *94*, 3123–3130. [CrossRef]
70. Liu, Q.; Chen, M.; Zheng, K.; Yang, Y.; Feng, X.; Li, H. In Situ Electrochemical Investigation of Pyrite Assisted Leaching of Chalcopyrite. *J. Electrochem. Soc.* **2018**, *165*, H813–H819. [CrossRef]
71. Weber, I.; Böttger, U.; Pavlov, S.G.; Hübers, H.W.; Hiesinger, H.; Jessberger, E.K. Laser alteration on iron sulfides under various environmental conditions. *J. Raman Spectrosc.* **2017**, *48*, 1509–1517. [CrossRef]
72. Venkataramanan, M.; Skanth, G.; Bandyopadhyay, K.; Vijayamohanan, K.; Pradeep, T. Self-assembled Monolayers of Two Aromatic Disulfides and a Diselenide on Polycrystalline Silver Films: An Investigation by SERS and XPS. *J. Colloid Interface Sci.* **1999**, *212*, 553–561. [CrossRef]
73. Ali Asaad, M.; Sarbini, N.N.; Sulaiman, A.; Ismail, M.; Huseien, G.F.; Abdul Majid, Z.; Bothi Raja, P. Improved corrosion resistance of mild steel against acid activation: Impact of novel Elaeis guineensis and silver nanoparticles. *J. Ind. Eng. Chem.* **2018**, *63*, 139–148. [CrossRef]
74. McGowan, G.; Prangnell, J. The significance of vivianite in archaeological settings. *Geoarchaeology* **2006**, *21*, 93–111. [CrossRef]
75. Morozov, Y.; Calado, L.M.; Shakoor, R.A.; Raj, R.; Kahraman, R.; Taryba, M.G.; Montemor, M.F. Epoxy coatings modified with a new cerium phosphate inhibitor for smart corrosion protection of steel. *Corros. Sci.* **2019**, *159*, 108128. [CrossRef]